Highly efficient CO 2 reduction under visible-light on noncovalent Ru•••Re assembled photocatalyst: evidence on the electron transfer mechanism

Houssein Nasrallah, Pengbo Lyu, Guillaume Maurin, Mohamad El-Roz

Highly efficient CO_2 reduction under visible-light on non-covalent Ru···Re assembled photocatalyst: evidence on the electron transfer mechanism

Houssein Nasrallah[a], Pengbo Lyu[b], Guillaume Maurin[b] and Mohamad El-Roz[a*]

a) Normandie Université, ENSICAEN, UNICAEN, CNRS, Laboratoire Catalyse et Spectrochimie, 14000 Caen, France.
b) ICGM, Univ. Montpellier, CNRS, ENSCM, Montpellier, France

Keywords: Artificial photosynthesis, CO_2 photoreduction, supramolecular assembly, electron transfer

ABSTRACT: Herein, two complexes: Pyrene modified photosensitizer (**RuPy**) and catalyst (**ReCOPy**) were synthetized and combined to form a novel bimetallic supramolecular assembly **RuPy**···**ReCOPy** via a combination of π-π stacking and hydrogen bond interactions. This supramolecular assembly was further characterized by electrochemical and spectroscopic techniques in order to determine its redox and photochemical properties. This novel **RuPy**···**ReCOPy** supramolecular assembly was demonstrated to display a high level of performance for the photocatalytic conversion of CO_2 conversion into CO with turn over frequency and CO quantum yield much higher (TOF: 18 h^{-1}, Φ_{CO}: 0.77) than the value obtained for the benchmark system $Ru(bpy)_3Cl_2$ (**Ru)** with $Re(bpy)(CO)_3Cl$ **(ReCO**) (5.3 h^{-1}, Φ_{CO} : 0.38). Time resolved spectroscopy and Density Functional Theory calculations revealed that an electron transfer mechanism is at the origin of the highly photocatalytic performance of **RuPy···ReCOPy**.

1. INTRODUCTION

In the recent years, the use of CO_2 as an alternative carbon source has become increasingly attractive for the production of useful carbon compounds, i.e. HCOOH, MeOH, CH_4 and CO, among others. [1-3] In particular, CO_2 reduction using photocatalysts to mimic the solar light driven photosynthesis is a topical subject. In this field, the photocatalytic systems envisaged so far are split into three categories: *i*- semiconductor systems, [4-8] *ii*- biohybrid systems [9-12] and *iii*- organometallic complexes. This later strategy was initiated by Lehn et *al.* in 1983 using $Re(bpy)(CO)_3Cl$ catalyst to convert CO_2 into CO. [13,14] A wide range of metal-based complexes, i.e. Ru, Rh, Co and Mn have been further demonstrated to show even higher photocatalytic activities for CO_2 conversion.[15,16] Generally, a photosensitizer (PS) is required in tandem with the co-catalyst (Cat) to enable absorption of visible light and transfer the electron from a sacrificial electron donor to the Cat. Typically, Ishitani *et al.* reported several supramolecular photocatalysts by covalent linking of different photosensitizers and co-catalysts. In these systems, an efficient and faster electron transfer (ET) via intramolecular process was demonstrated to impact substantially their catalytic performance. [17-25] A faster ET from the photosensitizer to the metallic center

of the catalyst reduces the undesirable deactivation process of the PS excited state. Reducing the distance between the PS and the Cat via non-covalent interactions is an alternative promising strategy developed recently for making the ET more efficient. This allows adjusting the PS/Cat ratio, simplifying the synthesis process comparing to covalently linked PS-Cat, expanding their use and adaptation with other PS/Cat moiety and/or their potential adsorption on conductive support, etc. In this context, Kubiak et *al.* reported, recently, intramolecular ET by assembling $Ru(dac)(bpy)_2(PF6)_2$ and $Re(dac)(CO)_3Cl$ (dac = 4,4′-bis(methyl acetamidomethyl)-2,2′-bipyridine, bpy = 2,2′-bipyridine) *via* (-NH---O=C-) hydrogen bond interactions resulting in a substantial improvement of the CO_2 conversion as compared to the combination of $Re(dac)(CO)_3Cl$ with the commercial $Ru(bpy)_3PF_6$.[26,27] Another system stabilized by π- π stacking interactions was reported, recently, by He et al, with Re[4,4′-di(pyren-1-yl)-2,2′-bipyridine]$(CO)_3Cl$ (4.4'-dipyrenyl-Re) as co-catalyst in the presence of $Ru(bpy)_3Cl_2$ enabling an efficient conversion of CO_2 into CO.[28] This intermolecular π-π stacking was found to boost ET leading to a turnover number (TON) twice higher than that obtained using the commercial $Re(bpy)CO_3Cl$. On the other hand, the 4.4'-dipyrenyl-Re was active for CO_2 photoreduction without the photosensitizer under solar light. This led to a light harvesting enhancement due to the π- π conjugation between the pyrene and the bipyridine groups of the catalyst as well as to the accelerated intermolecular ET through the stacked pyrenes. Very recently, Lu *et al.* reported a series of $Ru(Phen)_3^{2+}$ complexes (Phen: 1, 10-Phenanthroline) modified by pyrene as photosensitizers in association with cobalt-complex based catalyst for CO_2 photoreduction.[29] The significant enhancement, observed with one of the modified photosensitizer, was assigned to an improvement of their photosensitization due to a long-lived excited state and suitable excited-state oxidation potential. It is also well documented that the π-π interactions enable the immobilization of pyrene modified catalysts on the surfaces of carbon allotropes for recycling purposes, i.e. reduced graphene oxide, carbon nanotubes and C60 among others. [30-34] Typically, Gray *et al.* reported the synthesis of a series of bipyridine-based complexes containing two pyrenes moieties to be immobilized on carbon electrode via π- π stacking for electrochemical CO_2 reduction. [35,36] Herein, we report two ruthenium and rhenium-based complexes, i.e. **RuPy** and **ReCOPy** respectively, containing both, two pyrenes linked via $-CH_2$-NH-CO- bonds with the bipyridine moieties (**Fig. 1**). The so-designed complexes are assembled to produce a photocatalytic supramolecular PS/Cat system via an unconventional combination of π-π stacking and hydrogen bond interactions. In addition to the short separating distance between PS and Cat, we demonstrated that the π-π stacking promotes an efficient ET mediated by the pyrene moieties to achieve an outstanding conversion of CO_2 under visible light. Time resolved photoluminescence experiments were further combined with Density Functional Theory (DFT simulations) to shed light into the efficient electron transfer at the origin of the remarkable performances of this novel supramolecular photocatalytic system.

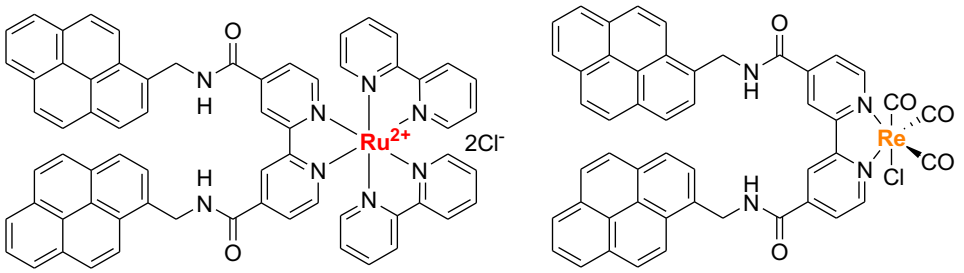

RuPy **ReCOPy**

Fig. 1. ReCOPy and **RuPy** complexes combined in this work to design a novel supramolecular assembly via hydrogen bond and π-π stacking.

2. EXPERIMENTAL SECTION

2.1. Materials

1,8-diazabicyclo[5.4.0]undec-7-ene (DBU), 4,4'-Dimethyl-2,2-bipyridine and the complex $Re(bpy)(CO)_3Cl$ were purchased from TCI chemicals. $Ru(bpy)_2Cl_2.6H_2O$, $Ru(bpy)_3Cl_2$, $ReCO_5Cl$, DMF, $SOCl_2$ and 1-pyrenemethylamine hydrochloride were purchased from Merck company. Commercially available acetonitrile, toluene, THF, DMF were used without any distillation.

2.2. Complexes RuPy and ReCOPy preparation

2.2.1. 4,4'-Dicarboxylic acid-2,2-bipyridine (HOOC-Bpy-COOH).

4,4'-Dimethyl-2,2-bipyridine (5.0 g) in heated H_2SO_4 (125 mL, 70-80 °C) was oxidized by adding solid potassium dichromate (24 g) slowly. The temperature was held consistently between 70 and 80 °C during the transfer. The deep green mixture was then poured over 800 mL of ice/ H_2O, affording a light-yellow precipitate that was isolated by vacuum filtration and was washed with H_2O. The solid was then refluxed in 50% HNO_3 (150 mL) for 4 h. The cooled solution was then poured over ice and diluted with 800 mL of H_2O. A white powder was isolated by vacuum filtration and washed with H_2O (5 g, 73%). ^1H NMR (400 MHz, DMSO-d_6) δ (ppm): 13.83 (2H, br s, R-COOH), 8.92 (d, J= 5.1 Hz, 2H), 8.85 (s, 2H), 7.92 (dd, J=4.9, 1.2 Hz, 2H).

2.2.2. $N^{4,4'}$-bis(1-pyrenylmethyl)-[2,2´-dipyridyl]-4,4´-dicarboxamide (Ligand-Bpy-Py).

The acid chloride of 2,2´- bipyridine-4,4´-dicarboxylic acid was prepared by refluxing 0.37 g (1.5 mmol) of the 4,4-dicarboxylic acid-2,2-bipyridine acid in 15 mL of thionyl chloride for 6 h. Remaining thionyl chloride was removed under vacuum. In a separate flask, 0.8 g (3 mmol) of 1-pyrenemethylamine hydrochloride were combined with 150 mL of dry acetonitrile and 0.9 mL of 1,8-diazabicyclo[5.4.0]undec-7-ene (DBU). The resulting solution was transferred to the solid bipyridine-acid chloride via cannula. The mixture was stirred for 12 h at room temperature, at which time 20 mL of saturated sodium bicarbonate and

130 mL of distilled water were added to form a beige precipitate. The precipitate was collected by filtration and washed with deionized water. The precipitate was dried under vacuum to give 0.62 g (61%) of an off-white solid. ^{1}H NMR (400 MHz, DMSO-d6) δ (ppm), 9.73 (t, J = 3.6 Hz, 2H), 8.86-8.84 (m, 4H), 8.51, (d, J= 6Hz, 2H), 8.34-8.26 (m, 9H), 8.18 (m, 5H), 8.13 (d, J= 5.3 Hz, 2H), 8.08 (t, J = 4.4 Hz, 2NHamide), 5.28 (d, J= 3.7 Hz, 4H).

2.2.3. $N^{4,4'}$-bis(1-pyrenylmethyl)-[2,2´-dipyridyl]-4,4´-dicarboxamide)-bis(2,2′-bipyridine dichloro ruthenium (II) (RuPy).

A solution of Ru(2,2′-bipyridine)$_2$Cl$_2$ (21 mg, 0.044 mmol) with **Ligand-Bpy-Py** (30 mg, 0.044 mmol) in 0.6 mL of DMF was refluxed 18 h at 153 °C under argon. The product was precipitated by addition of diethyl ether and sonicated during five minutes. The product was collected by centrifugation and washed with additional diethyl ether. The obtained solution was then dried by rotary evaporation to obtain 26 mg of dark red powder. (Yield = 50%) ^{1}H NMR (400 MHz, DMSO-d6) δ (ppm) 9.95 (t, J = 3.5 Hz, 2H), 9.40 (s, 2H), 8.83 (t, J = 5.2 Hz, 4H), 8.52 (d, J = 6.4 Hz, 2H), 8.33-8.23 (m, 9H), 8.20-8.12 (m, 9H), 8.09 (t, J = 5 Hz, 2H), 7.96-7.89 (m, 4H), 7.74 (d, J = 3.6 Hz, 2H), 7.68 (d, J = 3.6 Hz, 2H), 7.54-7.51 (m, 2H), 7.46-7.43 (m, 2H), 5.30 (d, J = 4.4 Hz, 4H). ^{1}H NMR (125 MHz, DMSO-d6) δ (ppm) 163.13 (CO), 157.67 (C_{IV}), 156.81(C_{IV}), 156.76 (C_{IV}), 152.52 (CH), 152.09 (CH), 151.53 (CH), 141.73 (C_{IV}), 138.67 (CH), 138.63 (C_{IV}), 132.57 (C_{IV}), 131.21 (C_{IV}), 130.71(C_{IV}), 130.69(C_{IV}), 128.60 (C_{IV}) 128.44 (CH), 128.41 (CH), 128.14 (CH), 127.83 (CH), 127.67 (CH), 126.77 (CH), 126.25 (C_{IV}), 125.81 (CH), 125.66 (CH), 125.21 (CH), 125.01 (CH), 124.48 (C_{VI}), 124.33 (C_{IV}), 123.87 (CH), 122.55 (CH), 41.74 (CH_2). ESI-MS (positive) m/z: found 542.14 (**RuPy**/2 − 2Cl), calculated 539.14 (**$RuC_{66}H_{46}N_8O_2$**)$^{2+}$.

2.2.4. *fac*-($N^{4,4'}$-bis(1-pyrenylmethyl)-[2,2´-dipyridyl]-4,4´-dicarboxamide)tricarbonylcholoro rhenium (I) (ReCOPy).

A solution of Re(CO)$_5$Cl (18 mg, 0.049 mmol) with **Ligand-Bpy-Py** (30 mg, 0.044 mmol) in 1 mL of toluene was refluxed 18 h at 110°C under argon. The solution was centrifuged to give an orange solid. The solid material was redissolved in THF before being centrifuged once more. The obtained solution was then concentrated and dried by rotary evaporation to obtain 30 mg of an orange precipitate. (Yield = 68%).^{1}H NMR (400 MHz, DMSO-d6) δ (ppm) 9.92 (t, J =3.7 Hz, 2H), 9.18 (d, J= 3.8 Hz, 2H), 9.12 (s, 2H), 8.46 (d, J= 6.1 Hz, 2H), 8.34-8.24 (m, 9H), 8.07-8.18 (m, J= 5.27Hz, 9H), 8.08 (t, J = 5 Hz, 2NH amide), 5.32 (d, J = 4 Hz, 4H). ESI-MS (positive) m/z: found 999.14 (**ReCOPyNa**), calculated 999.13 (**$ReC_{49}H_{30}N_4O_5ClNa$**).

2.3. Electrochemistry

Electrochemical measurements were realized with a PowerEase 300W Power Supply, 230 VAC. All experiments were performed in DMF, the supporting electrolyte was 0.1 M tetrabutylammonium

hexafluorophosphate ($TBAPF_6$), using a standard three-electrode configuration: 2 mm diameter. Platinum disk working electrode, a silver wire immersed in a solution of 0.1 M $TBAPF_6$ served as a reference electrode and the counter electrode was a Pt wire. The ferrocenium/ferrocene ($Fc^{+/0}$) couple was used as an external reference in all experiments to calibrate potentials. Voltammetry collected for solution-soluble redox couples with typically concentrations of 3×10^{-4} M with scan rate of 100 mV/s.

2.4. Photocatalytic tests

The photocatalytic CO_2 reduction was tested in an in-situ reactor developed in the LCS laboratory and presented in **Fig. S5**. The reactor is made from glass with horizontal tubes which ensuring the FTIR beam pathway through CaF_2 windows. The reactor is equipped with air circulator system for cooling and two gas inlet and outlet. The visible irradiation is ensured from the top through a removable quartz window. The quartz and CaF_2 windows are attached to the reactor with screw fittings and the tightness is obtained by adapted Teflon O-rings. The total internal volume of the reactor is 160 ± 5 ml. All IR spectrum measurements with the in situ FTIR reactor were monitored in real time with 5 min per spectrum of time resolution. IR spectra of the reactor headspace were recorded using Nicolet 6700 IR spectrometer (Thermo Fisher 14 Scientific) equipped with an MCT detector. All photocatalytic tests presented in this work were performed in batch configuration and at room temperature. As a light source, Xe-lamp 16 (LC8 Hamamatsu, 200 W) with pass-high filter at 390 nm was used. Complexes were dissolved in DMF/H_2O mixture (10/1.8 ml) and the solution was bubbled with saturated with CO_2 for one hour with a flow rate of 8 ml min^{-1}. Then, triethanolamine (TEOA) was introduced as electron donor (220 mg in 1 mL) in the reactor where the CO_2 bubbling was maintained for additional 15 minutes.

3. RESULTS AND DISCUSSION

3.1. Electro-photochemical characterizations

Two complexes were synthesized in this study, namely **ReCOPy** and **RuPy (Fig. 1c).** The first one was prepared according to the protocol reported in a previous study which considered this complex for the electro-catalytic reduction of CO_2. [36] **RuPy** was synthetized, for the first time in this work, from the equimolar mixture of $Ru(bpy)_2Cl_2$ and **Bpy-Py** ligand. The other two commercial homologues **Ru** and **ReCO** complexes were used for comparison.

The electrochemical analysis was performed in order to determine the redox potentials of the different systems. The cyclic voltammetry (CVs) of **Ru** and **ReCO** complexes agrees well with the literature. [27] A first reduction from Ru^{2+} to Ru^{+} and from Re^{+} to Re^{0} occurs at -1.77 V and at -1.79 V, respectively, with reversible oxidation bands at -1.71 V and -1.70 V, respectively **(Fig. 2)**. Regarding the **ReCOPy** complex, the reduction band of $\mathbf{ReCO^{+}/ReCO^{0}}$ is shifted to -1.96 V with a quasi-reversible oxidation band at -1.86V.

On the other hand, The CV analysis of the **RuPy** complex showed a first oxidation band of $\mathbf{RuPy^{2+}}$/ $\mathbf{RuPy^{+}}$ at -1.73V. In addition to the UV-visible absorption data (bad gap values), these reduction potential values will be used later for calculating the energetic positions of the HOMO (Highest Occupied Molecular Orbital) and LUMO (Lowest Unoccupied Molecular Orbital) of the corresponding complexes.

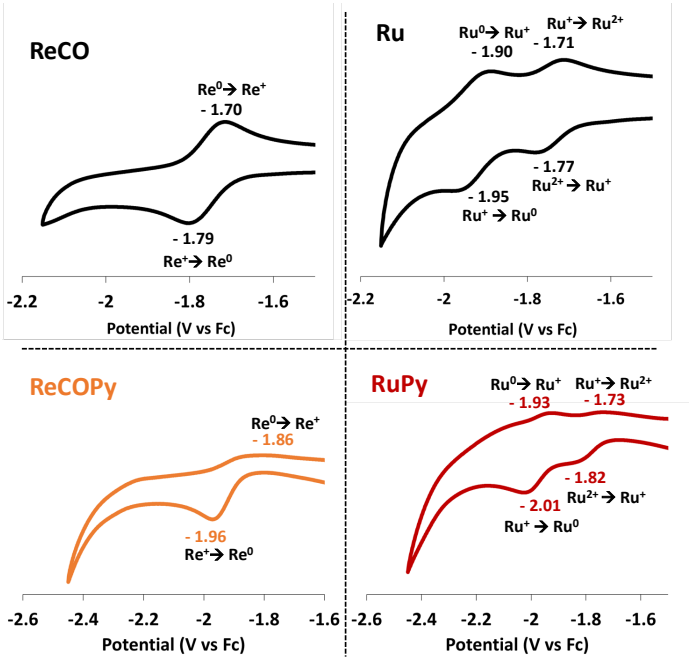

Fig. 2. Cyclic voltammetry for the **ReCO**, **ReCOPy**, **Ru** and **RuPy** complexes in DMF. Conditions: 100 mV/s, 0.1 M $TBAPF_6$, Pt working electrode, Pt wire counter electrode, Ag/AgCl reference electrode. Referred to ferrocenium/ferrocene couple.

The UV-Vis spectra of the complexes highlight the interaction of pyrene function with the metal center (**Fig. 3a**). The absorption bands, located at 458 nm and 370 nm for **Ru** and **ReCO**, respectively, are assigned to the metal to ligand charge transfer (MLCT). [37,38] However, a red-shift of ca. 20 nm is noted in MLCT absorbance range for both **RuPy** and **ReCOPy** complexes (478 and 405 nm, respectively). This red-shift consolidates the hypothesis of the electron delocalization between the metal center and the pyrene indicating strong interactions between them. It should be noted that no significant influence of the grafted pyrene group on the absorbance coefficient was observed in this work, in contrast to what has been observed when pyrene is directly linked to the bipyridine group of $Re(bpy)(CO)_3Cl$. [28] In the last case, a significant increase in the coefficient molar absorption of the MLCT is observed in addition to the red-shift. This difference can be explained by a higher delocalization of the electron between the directly-linked pyrene and the 4,4'-dipyrenyl-Regroup via a single bond**.** In contrast, the contribution of the pyrene in the electron delocalization is probably lower for **ReCOPy**, however the structure flexibility is higher owing to the presence of $-CH_2$-NH-CO- linker, which is more suitable, in our case, for promoting the desired interaction with **RuPy** photosensitizer. In order the investigate the interaction between **RuPy** and **ReCOPy,** a mixture of ratio 1:1

of complexes was analyzed by UV-Vis (**RuPy**···**ReCOPy**$_{exp}$) and the obtained spectra was compared with that of theoretical calculated from the addition of the individual **RuPy** and **ReCOPy** spectra (**RuPy**···**ReCOPy**$_{calc}$). (**Fig. 3b)** The subtraction of the two spectra **RuPy**···**ReCOPy**$_{exp}$-**RuPy**···**ReCOPy**$_{calc}$ indicates the presence of band-edge shifts with a modification in some band intensity. 321 and 339 nm resulting from the band-shift of pyrene at 330 and 345 nm, respectively. On the other hand, the characteristic bands 278 and 345 nm of pyrene was more intense in the **RuPy**···**ReCOPy**$_{exp}$ spectrum. In addition, a bleaching were observed at 473 and 350 nm and attributed to the MLCT and metal centered d-d transitions (MC), respectively. This bleaching is accompanied with a relative increase of the band intensity centered at 290 nm and assigned to π-π^* transitions (*LC) of the ligand. [39] These observations confirm the interaction between **RuPy** and **ReCOPy** in solution through the pyrene moieties which indicate a plausible formation of supramolecular assembly of **RuPy**···**ReCOPy**. It should be noted, that the relative low intensity due to the interaction could probably due to the fact of the **ReCOPy**···**ReCOPy** interaction. Therefore, the difference, is the additional impact of the **RuPy**···**ReCOPy** interaction in respect to the self-**ReCOPy** interaction.

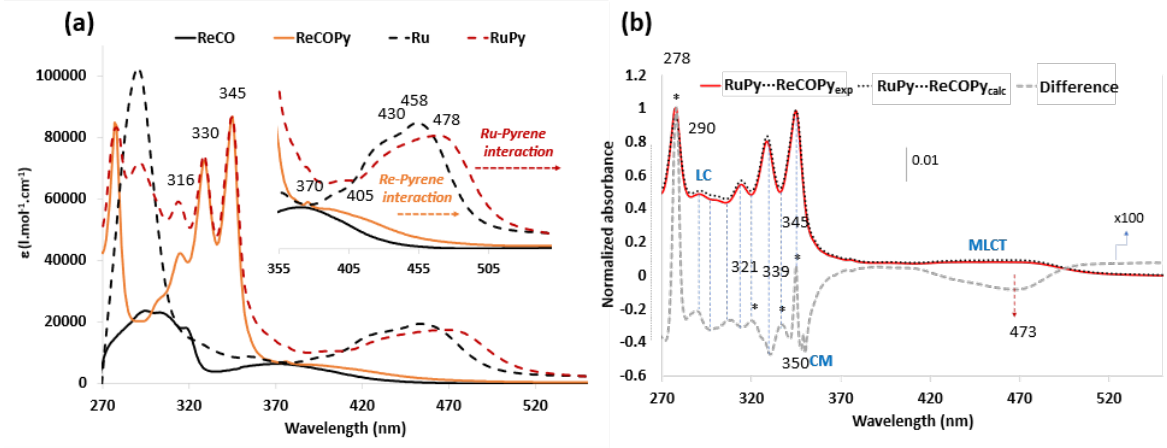

Fig. 3. (a) UV-Visible spectra of **Ru**, **RuPy** photosensitizers and of **ReCO**, **ReCOPy** co-catalysts in DMF. Insert: zoom on the region of the MLCT bands. (b) Normalized spectra of **RuPy-ReCOPy** (1:1) mixture (**RuPy-ReCOPy**$_{exp}$) and of mathematic addition of **RuPy** and **ReCOPy** (**RuPy**···**ReCOPy**$_{calc}$) with the difference between the two spectra, respectively. [**Ru**] = [**RuPy**] = [**ReCO**] = [**ReCOPy**] = 0.4 mM, [**RuPy**···**ReCOPy**$_{exp}$] : [**RuPy**] = [**ReCOPy**] = 0.2 mM *characteristic bands of pyrene

3.2. Photocatalytic performance.

All photocatalytic tests were carried out under similar visible light irradiation condition, in DMF, using triethanolamine (TEOA) as sacrificial electron donor and after saturation of the catalytic batch reactor with CO_2. The gas phase was monitored during the reaction by *in-situ* FTIR and the amount of CO produced was quantified following the characteristic bands at 2116 and 2171 cm^{-1} (**Fig. 4b**) as reported in our recent works. [40] It should be noted that the CO is formed selectively from the CO_2 reduction as demonstrate Figure S8

using labelled CO_2 ($^{13}CO_2$). All tests were reproduced at least two times and the error bars were estimated to be less than ±10% (**Fig. S9**). The reactor temperature was maintained at around 25°C by air cooling circuit. The selectivity toward CO vs HCOOH formation was >99% in all cases, under our reaction conditions as further confirmed by gas chromatography (**Fig. S9**).

An equimolar mixture of complexes **RuPy**···**ReCOPy** (1:1) was found to produce around 0.1 mmol of CO after one hour with an initial reaction rate V_0 of 0.12 mmol.h^{-1} and turn over frequency (TOF) of 18±2 h^{-1}. These results were compared to those obtained with the commercial **Ru** and **ReCO** complexes, tested under the same conditions. Remarkably, our new **RuPy**···**ReCOPy** s system shows a substantially higher activity with a TOF three times higher than the value obtained for **Ru**···**ReCO** (18 vs 5.3 h^{-1}, respectively) as well as four-fold higher initial reaction rate V_0 (0.12 vs 0.03 mmol.h^{-1}, respectively). (**Table S1**) Additionally, a very high quantum yield (Φ_{co}) for CO formation was calculated to be 0.77 for **RuPy**···**ReCOPy** and 0.38 in case of **Ru**···**ReCO** .Comparing the relative TOF and Φ_{co} with that reported in the literature when mononuclear homogeneous counterparts (PS + Cat) are used as reference allows ranking our system as one of the four most efficient counterpart systems reported in the literature (**Table S2).** This observation emphasizes a major role of the pyrene function on TOF and reaction rate in the photocatalytic process (**Fig. 4a**). However, the absorbance behaviors of the photosensitizers as well as the redox potentials of the different complexes cannot justify this gap between both systems. In order to better understand this performance, equimolar mixtures of PS (**Ru** or **RuPy**) and Cat (**ReCO** or **ReCOPy**) binary combinations were further explored and tested under similar conditions. The combination of **RuPy**···**ReCO** was tested with 1:1 ratio and surprising negligible activity was detected (TOF = 0.4 h^{-1}). Moreover, **Ru**···**ReCOPy** (1:1) showed **a** poor conversion (TOF = 2.2 h^{-1}) (**Fig. 4c**). These results seem contradictory to what has been reported recently on the benefit effect of the pyrene-modified photosensitizer [28,29] where a higher efficiency of **Ru**···**ReCOPy** systems (as well as for **RuPy**···**ReCO)** is expected with respect to **Ru**···**ReCO**. The very low activity indicates that ET between the pyrene modified **RuPy**/**ReCOPy** structures and unmodified **Ru**/**ReCO** structures are not favorable despite the suitable redox potentials of the different couples. The effect of PS:Cat ratio on the photocatalytic activity of the system was also investigated. The tests with different **RuPy**:**ReCOPy** ratios were performed under similar conditions and the results are reported in **Fig. 4d and S12**. A lower concentration of the PS or Cat (ratio 0.5:1 and 1:0.5) led to a significant decrease of the TOF (8.3 h^{-1} and 14.8 h^{-1} respectively). Moreover, a higher concentration of the photosensitizer (**RuPy:ReCOPy** 2:1) or of the catalyst (**RuPy**:**ReCOPy** 1:2) causes a dramatic drop of the performance (TOF = 13.4 h^{-1} and 7.9 h^{-1}, respectively). These observations are different from that obtained with a covalent supramolecular PS-Cat where the highest activities were observed with 1:3 and 1:2 of PS:Cat ratios. [41-43] In order to figure out the role of the linked pyrene function on the complexes, a complementary experiment was performed by adding free pyrene (4 equivalent relative to the PS) to the

RuPy···**ReCOPy** with the idea that free pyrene can interact with the pyrenes of the complexes and consequently minimize the possible π-π interactions between the **RuPy** and **ReCOPy** (It should be noted that free pyrene couldn't interfere with the light absorption in the visible irradiation range). As excepted, a decrease of the catalytic activity was observed **(Fig. 4c**), with two times lower TOF (8.2 h^{-1}) than that observed for pyrene-free system and close to that observed for **Ru**···**ReCO** complex used as reference.

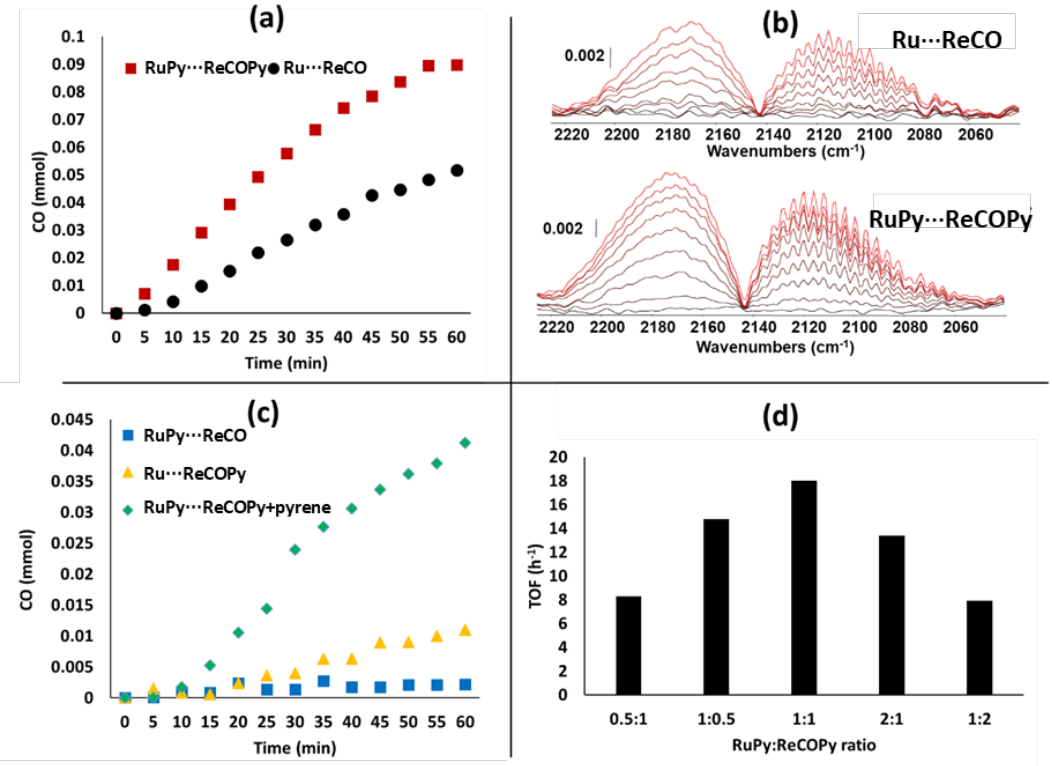

Fig. 4. Evolution of the CO amount during the photocatalytic reduction of CO_2 under visible light over: a) **RuPy**···**ReCOPy** and **Ru**···**ReCO**; c) **Ru**···**ReCOPy**, **RuPy**···**ReCO** and **RuPy**···**ReCOPy**+pyrene; d) Evolution of the TOF vs the ratio of **RuPy**:**ReCOPy**. b) Characteristic IR CO band evolutions in the first 30 minutes of irradiation for **RuPy**···**ReCOPy** and **Ru**···**ReCO**. Reaction condition: [**Ru**]=[**RuPy**]= 0.38 mM; [**ReCO**]=[**ReCOPy**)] = 0.38 mM; [TEOA]= 0.12 M; [H_2O] = 8.3 M; Vol_{DMF}= 11 ml; Xe-Lamp; Irradiance~10 mW/cm^2; Filter pass high for λ>390 nm; errors estimated lower than 10% on three reproducible experiments. TOFs were always based on the amount of Re complexes.

It to be noted that our new system **RuPy**···**ReCOPy** (1:1) displays a lower stability with respect to **Ru**···**ReCO** system in these conditions. A total deactivation was observed after ≈70 minutes (**Fig. S10**). In order to clarify the origin of this deactivation, a set of additional experiments was performed, e.g. the CO_2 purging and/or introduction of **RuPy** or **ReCOPy** moiety after the total deactivation. We evidenced that the activity can be only recovered by adding a fresh Cat (**ReCOPy**) to the solution showing that the degradation or the poisoning of this Cat is the only responsible of the deactivation process (**Fig. 5a**). However, the synergistic increase of the activity after adding "fresh" **RuPy** to solution containing only **ReCOPy,** and

previously irradiated for 240 minutes under CO_2 atmosphere in presence of TEOA, discarded the hypothesis of the catalyst photo-degradation (**Fig. 5b**). Therefore, the poisoning of this latter seems to be more realistic and probably due to the formation of a sub-product obtained from a possible reaction of the catalyst with the sub-product of electron donor (e.g. $TEOA^{\bullet}$). [44]. These experiments highlighted further the nature of the **RuPy/ReCOPy** interactions. The synergistic activity observed after adding the fresh **ReCOPy** to **RuPy**···**ReCOPy** or **RuPy** to the **ReCOPy** revealed the reversibility and the advantage of the non-covalent nature of the interactions between the PS and the Cat.

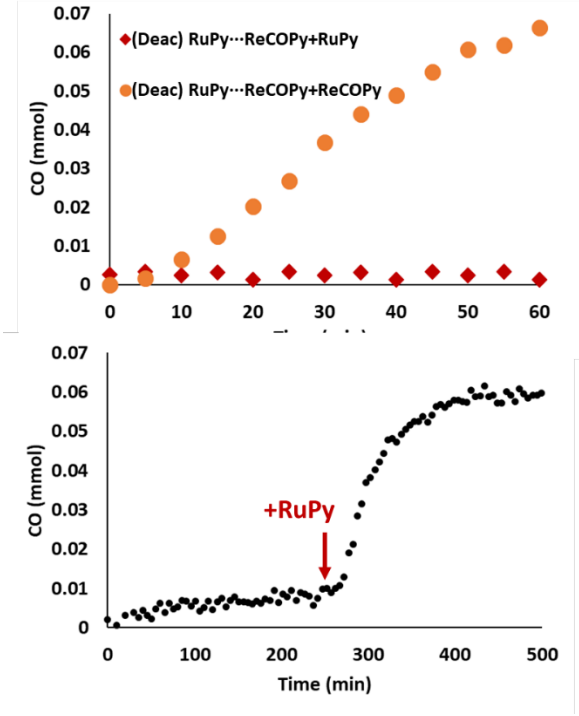

Fig. 5. a) Evolution of the CO amount during the photocatalytic reduction of CO_2 after 2 hours of bubbling CO_2 on deactivated **RuPy**···**ReCOPy** system and adding of **RuPy** and **ReCOPy**. (b) Evolution of the CO amount during the photocatalytic reduction of CO_2 over **ReCOPy** system before and after adding (indicated with arrow) of **RuPy** photosensitizer.

3.3. Time resolved emission of ^{3}MLCT and ^{3}IL excited state of PS.

Adjusting the excited-state lifetime of the photosensitizers is a key factor for an efficient reduction of CO_2 over PS/Cat system. Hence, the excited-state properties of **Ru** and **RuPy** were explored by measuring the time resolved photoluminescence (TR-PL) and absorption transient (AT) (**Fig. 6**). The PL of **Ru** and **RuPy** were significantly quenched as exposed to air (**Fig. 6a**), indicating the phosphorescence emission process, which mainly derived from the triplet state.[45] The TR-PL spectrum of **Ru** showed a typical ^{3}MLCT emission at 620 nm in DMF (**Fig. 6a**; **Fig. S13**). The ^{3}MLCT emission of **RuPy** is centered at 670 nm (**Fig. 6b**, **Fig. S13**), red-shifted for 50 nm with respect to **Ru**. This red-shift confirms the strong electrostatic interactions

between the Ru-center and pyrenyl, in agreement with the UV-visible absorbance results. These results are confirmed by the absorption transient. For the **Ru** (**Fig. 6c**), absorption transient (AT) bands centred at 370 nm, and 560 nm and assigned to T_1 and T_2 transients, respectively are observed, with λ_{exc}=532nm (as well as with λ_{exc}=355nm), with a similar kinetic decay of the bleaching (at 450-460 nm, 630 and 660 nm). For **RuPy**, the corresponding AT bands are red-shifted, in agreement with the PL and UV-visible absorbance, and centered at 380 nm and 570 nm with a similar kinetic decay of the bleaching (at 450-480 nm, 670 and 710 nm). The bleaching in the 600-700 nm region is mainly assign to the phosphorescence emission due to radiative relaxations of the triplet state. The lifetimes of the PL, AT and bleaching are very close for **Ru** as well as for **RuPy**. The kinetic decay trace of the **RuPy**'s PL and AT revealed 1.3-1.5 times higher excited-state lifetime than that of ^{3}**Ru** for a similar concentration (1.08-1.30 µs vs 0.75-0.90 µs, respectively). The ^{3}**RuPy** was also demonstrated to be 2.5 times less sensitive toward O_2 (**Table 1**). More surprising, a new distinctive AT band at 520 nm was selectively observed for **RuPy** with a longer lifetime of 35 µs (Insert of **Fig. 6d**). The sensitivity of this AT toward oxygen confirms that it corresponds to a triplet state and can probably be correlated to a formation of an exciplex ^{3}(**RuPy**···**RuPy**) and/or to an intermolecular charge separation. Moreover, the quenching of ^{3}**RuPy** by TEOA was found 2.8 times higher than that for ^{3}**Ru** (2.11×10^6 $M^{-1}s^{-1}$ vs 7.4×10^5 $M^{-1}s^{-1}$, respectively), indicating a faster electron transfer from the electron donor to the **RuPy**. It should be noted that the quenching rate constants calculated from the emission (Fig S11) are very similar to that calculated from the AT. A characteristic shoulder with a very short lifetimes (<10 ns) was selectively observed for **RuPy** (**Fig. S13a**), representative of a dual emission emerged in the PL spectrum. The PL emission spectra of **RuPy** after excitation at 355 nm confirmed this inspection (**Fig. S13b-d**) with additional emissions centred at 400 nm and 520 nm. This emission could be assigned to the pyrene moiety. Consequently, PL studies of pyrene molecule and of the **RuPy**'s ligand were performed. The PL measurement results indicated that this emission corresponds to the intra-ligand triplet excited state (^{3}IL). Therefore, observing this ^{3}IL upon 532 nm excitation (no absorption of pyrene and the ligand at 532 nm) substantiates the electron/energy transfer between the Ru-center to the pyrene part. The significant decrease of the ^{3}IL lifetime of pyrene (Py), in the following order **Py**(200ns)<**ReCOPY**(120 ns)<**Bpy-Py**(100 ns)<**RuPy**(85ns), confirms this assumption (**Fig. S13g**).

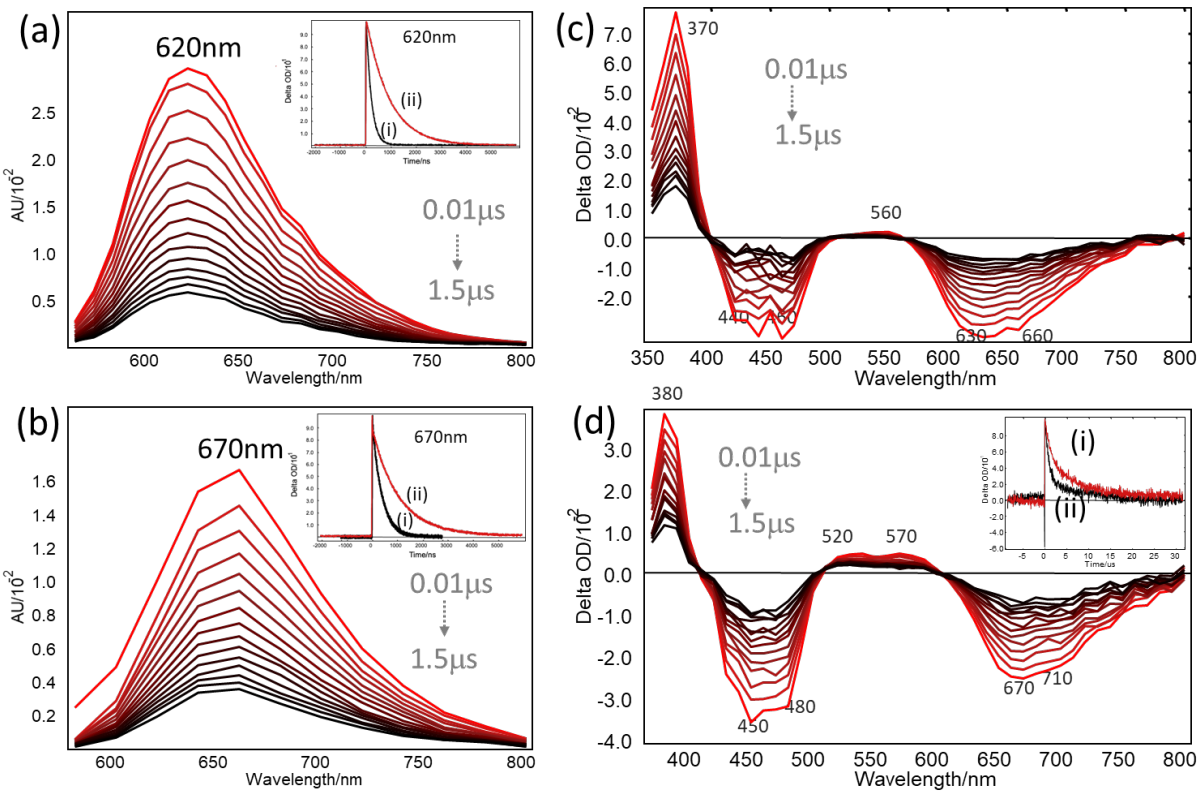

Fig. 6. (a) and (b) correspond to the nanosecond emission spectra (140ns/spectrum) of the ^{3}MLCT of **Ru** and **RuPy**, respectively. In insert: normalized kinetic decay trace of ^{3}MLCT emission of **Ru** and **RuPy** monitored at 620 nm and 670 nm, respectively, under air (i) and argon (ii) atmospheres. **(c)** and **(d)** report the evolution vs the time (140ns/spectrum) of the absorption transition (AT) of **Ru** and **RuPy**. Insert of Fig. d: normalized kinetic decay traces of the AT at 520 nm (i) and 570 nm (ii). λ_{exc} = 532 nm, [**RuPy**]=1.7 mM; [**Ru**]= 3 mM; all spectra were recorded under Ar at 298K.

We should keep in mind that the electron transfer is promoted only after the reduction of the ^{3}PS to PS$^-$ which is achieved by an electron transfer from the electron donor to the ^{3}PS. Therefore, other quenching process can also play a role in the decrease of this transfer as ^{3}PS-^{3}PS self-quenching and ^{3}PS-Cat quenching. The different rate constants of the ^{3}MLCT quenching of the **Ru** and **RuPy** are reported in **Fig. S14** and summarized in **Table 1**. Interestingly, the self-quenching of ^{3}**RuPy** is three times lower than that of ^{3}**Ru**. However, the quenching of ^{3}MLCT of **Ru** by **ReCOPy** is 500 times higher with respect to ^{3}**Ru**/**ReCO**. This quenching is in part promoted by the pyrene-moiety as demonstrated from the rate constant of the ^{3}**Ru** with pyrene (Table 1). The ^{3}**Ru**/Py quenching is 6 times higher than that for ^{3}**RuPy**/Py (and much higher than that the ET from TEOA), which could explain the very low activity of **Ru**/**ReCOPy** dual system. However, despite the low quenching rate of the ^{3}MLCT of **RuPy** by pyrene, the lifetime of ^{3}Py is dramatically affected with similar quenching rate constant founded with ^{3}**Ru**. This outweighs on a π-π interaction between the pyrene-moiety of **RuPy** with pyrene. On the other hand, the quenching of the ^{3}MLCT of **RuPy** by **ReCO** is four times lower than that with **ReCOPy** which could not explain the very low efficiency of **RuPy**/**ReCO**

binary system compared to **RuPy/ReCOPy**. The different data allow building the energetic diagram of the HOMO and LUMO, for the different complexes (see ESI for more details) as well as the energetic levels of the different excited states (basing on the AT experiments) of the **Ru** and **RuPy** photosensitizers (**Fig. S15**). It should be noted that the electron transfer occurs from the reduced photosensitizer *(PS$^{\bullet-}$), to the catalyst. The *(PS$^{\bullet-}$) is formed from the oxidation of the electron donor and the ^{3}PS. Therefore, a longer lifetime of **RuPy** excited state(s) is highly desired as well as a lower quenching is critical for promoting the ET from the TEOA to the ^{3}PS as well as from the reduced ^{3}PS$^{\bullet-}$ to the Cat. Consequently, the higher lifetime of the **RuPy**'s excited-state and its lower quenching with respect to that of **Ru** can justify, in part, the highest activity of the **RuPy**···**ReCOPy** system (in comparison to **Ru**···**ReCO**). However, this cannot explain the gap in the performance between **RuPy**···**ReCOPy** and **RuPy**···**ReCO**, where the energetic diagram reveals similar LUMO levels of **ReCO** with respect to **ReCOPy**. Therefore, other factors should be taken into account to elucidate this phenomenon.

Table 1. Stern–Volmer-quenching constants with **Ru** and **RuPy** measured at 298K from the PL kinetic decays at 620 nm and 650 nm, respectively, in presence of different quencher.

PS / Q	^{3}**Ru**$^{(a)}$	^{3}**RuPy**$^{(b)}$
	k_q x 10^8(M^{-1} s^{-1})	k_q x 10^8(M^{-1} s^{-1})
O_2	299	117
Ru/RuPy$^{(c)}$	4.47	1.71
ReCOPy	14.10	2.90
ReCO	0.07	0.55
TEOA	0.0021	0.0027
Py	5.19 ($13.1^{(d)}$)	0.87 ($11.0^{(d)}$)

(a) $\lambda_{emission}$=620nm; (b) $\lambda_{emission}$=650nm; (c) rate constant of the ^{3}**Ru**/^{3}**Ru** or ^{3}**RuPY**/^{3}**RuPy** self-quenching. λ_{exc}=532 nm; (d) rate constant of the ^{3}Py-moiety quenching of ($\lambda_{emission}$=400nm; λ_{exc}=355 nm). Error estimated at 5%.

3.4. Molecular Insight into the preferential arrangements of the PS/Cat systems

DFT calculations were performed on the different PS/Cat systems to identify the nature and strength of interactions between their constitutive components (see computational details in ESI). The geometry of the **Ru**···**ReCO**, **RuPy**···**ReCO**, **Ru**···**ReCOPy, ReCOPy**···**ReCOPy** and **RuPy**···**ReCOPy** systems were DFT-optimized using the Becke Three-Parameter Hybrid exchange functional [46] with the Lee-Yang-Parr correlation functional [47] (B3LYP) implementing the empirical dispersion function (D3) [48] and

associated with a triple zeta basis set TZVP [49] (except for Ru and Re which were described using the LANL2DZ basis set). [50] Other computational details can be found in ESI. Their corresponding most stable conformations are reported in **Fig. S16-S22**) and their associated PS/Cat interaction energies (E_{int}) are summarized in **Table 2**.

Table 2. Summary of the DFT-calculated interaction energy (E_{int}) for the different systems (expressed in kJ mol^{-1}). The interaction energy between the two components of each system was calculated as E_{int}=E(system)-E(complex 1)-E(complex 2) where E(system) is the total energy of the system assembling the two complexes 1 and 2 while E(complex 1) and E(complex 2) are the total energies of complex 1 and 2 taken individually, respectively. (1) and (2) correspond to two possible geometries for the **ReCOPy**/**RuPy** system, (1) being the most energetically favorable one. The determination of the interaction energy for the **RuPy**-**RuPy** system was not performed since we used a charged cation model to treat **RuPy**.

System	E_{int} (kJ mol^{-1})
Ru···**ReCO**	-156
RuPy···**ReCO**	-190
Ru···**ReCOPy**	-195
ReCOPy···**ReCOPy**	-261
RuPy···**ReCOPy (1)**	-295
RuPy···**ReCOPy (2)**	-227

These calculations revealed two plausible geometries for our new **RuPy**···**ReCOPy** system (labeled 1 and 2 in **Table 1**) as illustrated in **Fig. 7a** and **7b**. The configuration (1) corresponds to the most energetically stable geometry resulting from the N-H/C=O hydrogen bond (d ≈ 1.9 Å) and the bipyridine-pyrene π-π stacking (d ≈ 2.8 Å) between the PS and the Cat leading to the supramolecular assembly. In addition, a remarkable intramolecular alignment of pyrene functions can be clearly observed and assigned to an intramolecular π-π stacking (d ≈ 3.4 Å). The configuration (2) is less stable and corresponds to a supramolecular assembly stabilized mainly via inter- and intra-molecular pyrene–pyrene π-π stacking (d ≈ 3.4 Å) as well as a N-H/C=O hydrogen bonds (d ≈ 1.9 Å); however, in contrast to configuration (1), the bipyridine-pyrene π-π stacking interactions are absent. These configurations 1 and 2 are associated with interaction energies between **RuPy** and **ReCOPy** (-295 and/or -227 kJ.mol^{-1} respectively) significantly higher than the value obtained between **Ru** and **ReCO** in the respective complex (-156 kJ mol^{-1}). This result highlights that the introduction of pyrene in both **Ru** and **ReCO** leads to a substantial enhancement of the intermolecular interactions between the PS and Cat. These interactions energies are also significantly higher than the values calculated for **Ru**···**ReCOPy** (-195 kJ.mol^{-1}) and **RuPy**···**ReCO** (-190 kJ.mol^{-1}) (Table 2 and **Fig. S17** and **S18**) confirming the synergistic role played by the pyrene functions present in both PS and Cat. The interaction energy for the **ReCOPy**···**ReCOPy** complex (-261 kJ.mol^{-1}) was also found to be much

higher than the value obtained for **Ru**···**ReCOPy** (-195 kJ.mol^{-1}). This implies that the interactions between the **ReCOPy/ReCOPy** via intermolecular π-π stacking are stronger than that between the **Ru** and **ReCOPy** in the **Ru**···**ReCOPy** system (**Fig. S18**). Moreover, noting that the interaction energy for **ReCOPy**···**ReCOPy** (-261 kJ.mol^{-1}) is lower than the value calculated for **RuPy**···**ReCOPy** (-295 kJ.mol^{-1}) and the activity of **ReCOPy** is relatively poor without the introduction of **RuPy** (**Fig. 5b**), it comes that the 1:1 ratio maximizes the catalytic activity (**Fig. 4d**), otherwise excess of **ReCOPy** (and very likely **RuPy** as well) can group up and act similarly to the situation of **ReCOPy** only, decreasing therefore the activity.

The possible electron transfer (ET) pathway for the most energetically stable **RuPy**···**ReCOPy (1)** was further explored by time-dependent DFT (TD-DFT) calculations (see ESI for computational details). These calculations did not reveal any charge transfer from the ground state of ***RuPy**$^{\bullet-}$ to **ReCOPy**'s (see SI: **Fig. S19** and **table S4**) as we would have expected for the associated dark reaction. Only for the second excited state, a Mulliken absolute charge difference (Δq) was obtained for the ***RuPy**$^{\bullet-}$ (+0.0045 |e|) and **ReCOPy** metal centers (-0.0010 |e|) with the ground state considered as a reference.

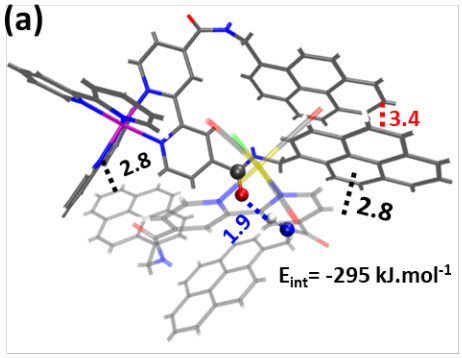

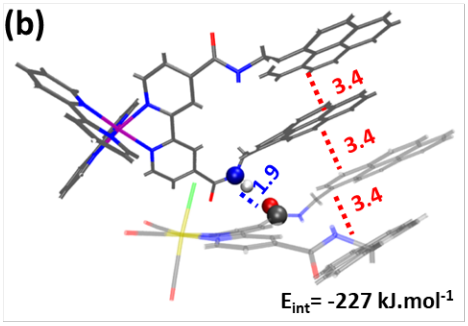

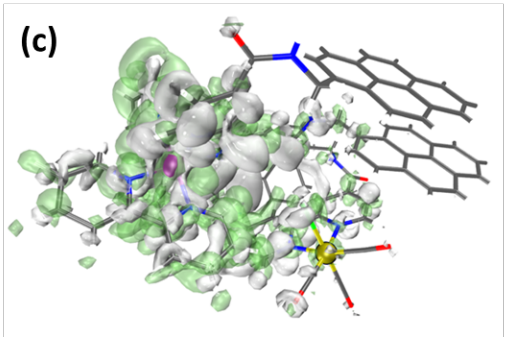

Fig. 7. DFT-calculations on the **RuPy**···**ReCOPy** system: a) the most stable configuration **(1)**, b) plausible configuration **(2)** and c) charge differences for the most stable **RuPy**···**ReCOPy (1)** complex upon the excitation to the second excited state. Green and white colors represent the charge accumulation and depletion regions respectively. Color code: carbon(grey), hydrogen (white), nitrogen (blue), (green), oxygen (red), ruthenium (purple) and rhenium (yellow). The distances are reported in Å.

3.5. Mechanistic investigation

After discarding the absorbance impact in the enhancement of the activity of **RuPy**···**ReCOPy** vs **Ru-ReCO** and based on the tests with other binary systems' combinations (**Fig. 4** and **S10**), on the excited-state lifetimes, on the quenching rate constant and on the DFT calculations, we concluded that the higher activity is mainly attributed to a faster ET between **RuPy** and **ReCOPy**. The modelling shows two possible pathways as illustrated in **Fig. 8**: (i) Following a preliminary MLCT from ruthenium center to the bipyridine (bpy) and the electron then migrates from the pyrene towards the bipyridine-rhenium center to trigger the CO_2 photoreduction; (ii) The electron migrates from the bipyridine of **RuPy** towards the pyrene moieties of Re and reaches the bipyridine-rhenium center after an intermolecular transfer (**Fig. 8**). The interaction energy calculated by DFT between the two complexes (**Table 2**) allows investigating the pathway (ii) as preferential. However, pathway (i) cannot be discarded since the DFT calculations did not take into account other factors such as the solvation effect. Consequently, with the stronger interaction between **RuPy** and **ReCOPy**, both ET pathways can occur simultaneously and/or separately for ensuring a fast ET.

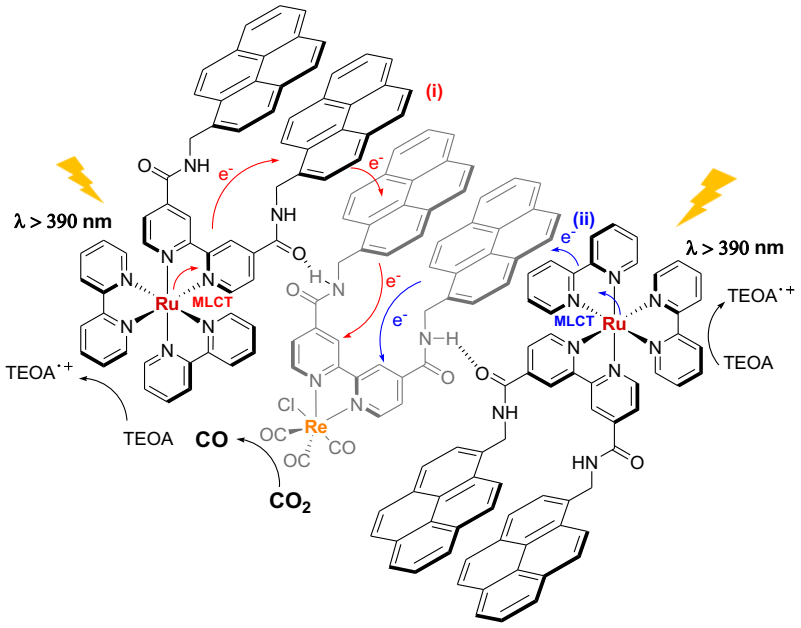

Fig. 8. The two possible electron pathways in the **RuPy**···**ReCOPy** photocatalytic systems based on the analysis of the experimental and theoretical data.

4. CONCLUSION

The newly designed **RuPy**···**ReCOPy** supramolecular photocatalytic system was demonstrated to show an enhanced conversion efficiency of CO_2 to CO under visible light. This supramolecular assembly is promoted by non-covalent NH/CO hydrogen bond and π-π staking interactions between the catalyst and the photosensitizer. Remarkably, the calculated TOF was found three times higher than the value previously reported for the conventional **Ru**···**ReCO** photocatalytic system (18 h^{-1} vs 5.3 h^{-1}). These reaction rates and photocatalytic activity enhancement is due to an efficient electron transfer from **RuPy** to **ReCOPy** mediated by the pyrene moieties and the stronger interactions between **RuPy** and **ReCOPy** as compared to **Ru** and **ReCO**. The electron delocalization between the pyrene moieties and the complexes was confirmed by UV-Vis study and TR-PL showing the electron transfer pathway from ruthenium center to the pyrene moiety in **RuPy** and from the pyrene moiety to the rhenium center in **ReCOPy**. Additionally, the faster electron transfer from the electron donor to the **RuPy** comparing with **Ru** was also concluded form the quenching of the ^{3}MLCT with TEOA. These findings shed light on the importance of the electron transfer efficiency and pathway for enhancing the performance of the photo-catalytic system for the CO_2 photoreduction.

Acknowledgements

This work is supported by European Regional Development Fund (ERDF), Normandy region, as part of the project: RAPHYD (*Recherche pour les Applications Energétiques de l'Hydrogène*). We thank Mr. Adel

Noon for his participation in this work during his internship and Mr. Adrien Lanel for In-situ FTIR reactor designing. This work was granted access to the HPC ressources of CINES under the allocation A0100907613 made by GENCI.

Supplementary materials

The following information are available in ESI: Ligand and complexes synthesis, NMR data, details for photocatalytic tests (in-situ reactor, calibration curve for CO quantification, FTIR spectra…), additional times resolved photoluminescence results (nanosecond emission and AT spectra, Stern-Volmert plots), energy level of HOMO and LUMO determination details and all optimized structure are presented in **Fig. S1-S22** and **Table S1-S5**.

References

[1] X. Li, J. Yu, M. Jaroniec, X. Chen, Cocatalysts for selective photoreduction of CO_2 into solar fuels, Chem. Rev. 119 (2019) 3962–4179. https://doi.org/10.1021/acs.chemrev.8b00400.
[2] A. Corma, H. Garcia, Photocatalytic reduction of CO_2 for fuel production: possibilities and challenges, J. Catal. 308 (2013) 168–175. https://doi.org/10.1016/j.jcat.2013.06.008.
[3] M. Aresta, A. Dibenedetto, A. Angelini, Catalysis for the valorization of exhaust carbon: from CO_2 to chemicals, materials, and fuels. Technological use of CO_2, Chem. Rev. 114 (2014) 1709–1742. https://doi.org/10.1021/cr4002758.
[4] Y. Sohn, H. Weixin, T. Fariborz, Recent progress and perspectives in the photocatalytic CO_2 reduction of Ti-oxide-based nanomaterials, App. Surf. Sci. 396 (2017) 1696−1711. https://doi.org/10.1016/j.apsusc.2016.11.240.
[5] N. Shehzad, M. Tahir, K. Johari, T. Murugesan, M. Hussain, A critical review on TiO2 based photocatalytic CO_2 reduction system: Strategies to improve efficiency, J. CO_2 Util. 6 (2018) 98−122. https://doi.org/10.1016/j.jcou.2018.04.026.
[6] D. Sánchez-Rodríguez, A. B. Jasso-Salcedo, N. Hedin, T. L. Church, A. Aizpuru, V. A. Escobar-Barrios, Semiconducting Nanocrystalline Bismuth Oxychloride (BiOCl) for Photocatalytic Reduction of CO_2, Catalysts, 10 (2020) 998. https://doi.org/10.3390/catal10090998.
[7] R. Liu, Z. Chen, Y. Yao, Y. Li, W. A. Cheema, D. Wang, S. Zhu, Recent advancements in gC_3N_4-based photocatalysts for photocatalytic CO_2 reduction: a mini review, RSC Adv. 10 (2020) 29408–29418. https://doi.org/10.1039/D0RA05779G.
[8]W. J. Ong, L. K. Putri, A. R. Mohamed, Rational Design of Carbon-Based 2D Nanostructures for Enhanced Photocatalytic CO_2 Reduction: A Dimensionality Perspective, Chem. Eur. J. 26 (2020) 9710–9748. https://doi.org/10.1002/chem.202000708.
[9] R. K. Yadav, J. O. Baeg, G. H. Oh, N. J. Park, K. J. Kong, J. Kim, D. W. Hwang, S. K. Biswas, A photocatalyst–enzyme coupled artificial photosynthesis system for solar energy in production of formic acid from CO_2, J. Am. Chem. Soc. 134 (2012) 11455–11461. https://doi.org/10.1021/ja3009902.
[10] Y.S. Chaudhary, T.W. Woolerton, C.S. Allen, J.H. Warner, E. Pierce, S.W. Ragsdale, F.A. Armstrong, Visible Light-driven CO_2 Reduction by Enzyme Coupled CdS Nanocrystals, Chem. Commun. 48 (2012) 58–60. https://doi.org/10.1039/C1CC16107E.
[11] Y. Chen, P. Li, J. Zhou, C. T. Buru, L. Đorđević, P. Li, X. Zhang, M. M. Cetin, J. F. Stoddart, S. I. Stupp, M. R. Wasielewski, O. K. Farha, Integration of enzymes and photosensitizers in a hierarchical mesoporous metal–organic framework for light-driven CO_2 reduction. J. Am. Chem. Soc. 142 (2020) 1768–1773. https://doi.org/10.1021/jacs.9b12828.
[12] A. Miyaji, Y. Amao, Artificial co-enzyme based on carbamoyl-modified viologen derivative cation radical for formate dehydrogenase in the catalytic CO_2 reduction to formate, New J. Chem. 44 (2020) 18803–18812. https://doi.org/10.1039/D0NJ04375C.
[13] J. Hawecker, J. M. Lehn, R. J. Ziessel, Efficient photochemical reduction of CO_2 to CO by visible light irradiation of systems containing Re(bipy)$(CO)_3$X or Ru(bipy)$_3^{2+}$–Co^{2+} combinations as homogeneous catalysts, Chem. Soc., Chem.Commun. (1983) 536−538. https://doi.org/10.1039/C39830000536.

[14] J. Hawecker, J. M. Lehn, R. J. Ziessel, Electrocatalytic reduction of carbon dioxide mediated by Re(bipy)$(CO)_3$Cl (bipy= 2, 2′-bipyridine), Chem. Soc., Chem. Commun. (1984) 328−330. https://doi.org/10.1039/C39840000328.
[15] D. Li, M. Kassymova, X. Cai, S. Q. Zang, H. L. Jiang, Photocatalytic CO_2 reduction over metal-organic framework-based materials, Coord. Chem. Rev. 412 (2020) 213626. https://doi.org/10.1016/j.ccr.2020.213262.
[16] Y. H. Luo, L. Z. Dong, J. Liu, S. L. Li, Y. Q. Lan, From molecular metal complex to metal-organic framework: the CO_2 reduction photocatalysts with clear and tunable structure, Coord. Chem. Rev. 390 (2019) 86−126. https://doi.org/10.1016/j.ccr.2019.03.019.
[17] R. Kamata, H. Kumagai, Y. Yamazaki, G. Sahara, O. Ishitani, Photoelectrochemical CO_2 Reduction Using a Ru(II)-Re(I) Supramolecular Photocatalyst Connected to a Vinyl Polymer on a NiO Electrode, ACS Appl. Mater. Interfaces 11 (2019) 5632−5641. https://doi.org/10.1021/acsami.8b05495.
[18] K. Koike, D. C. Grills, Y. Tamaki, E. Fujita, K. Okubo, Y. Yamazaki, M. Saigo, T. Mukuta, K. Onda, O. Ishitani, Investigation of excited state, reductive quenching, and intramolecular electron transfer of Ru(II)-Re(I) supramolecular photocatalysts for CO_2 reduction using time-resolved IR measurements, Chem. Sci. 9 (2018) 2961−2974. https://doi.org/10.1039/C7SC05338J.
[19] H. Kumagai, G. Sahara, K. Maeda, M. Higashi, R. Abe, O. Ishitani, Hybrid Photocathode Consisting of $CuGaO_2$ p-Type Semiconductor and a Ru(II)-Re(I) Supramolecular Photocatalyst: Non-Biased Visible-Light-Driven CO_2 Reduction with Water Oxidation, Chem. Sci. 8 (2017) 4242−4249. https://doi.org/10.1039/C7SC00940B.
[20] Y. Kuramochi, O. Ishitani, Iridium(III) 1-Phenylisoquinoline Complexes as a Photosensitizer for Photocatalytic CO_2 Reduction: A Mixed System with a Re(I) Catalyst and a Supramolecular Photocatalyst, Inorg. Chem. 55 (2016) 5702−5709. https://doi.org/10.1021/acs.inorgchem.6b00777.
[21] S. Sato, K. Koike, H. Inoue, O. Ishitani, Highly efficient supramolecular photocatalysts for CO_2 reduction using visible light, Photochem. Photobiol. Sci. 6 (2007) 454−461. https://doi.org/10.1039/B613419J.
[22] Y. Tamaki, O. Ishitani, Supramolecular Photocatalysts for the Reduction of CO_2, ACS Catal. 7 (2017) 3394−3409. https://doi.org/10.1021/acscatal.7b00440.
[23]Y. Tamaki, K. Koike, T. Morimoto, Y. Yamazaki, O. Ishitani, Red-Light-Driven Photocatalytic Reduction of CO_2 using Os(II)-Re(I) Supramolecular Complexes, Inorg. Chem. 52 (2013) 11902−11909. https://doi.org/10.1021/ic4015543.
[24] Y. Tamaki, K. Watanabe, K. Koike, H. Inoue, T. Morimoto, O. Ishitani, Development of highly efficient supramolecular CO_2 reduction photocatalysts with high turnover frequency and durability, Faraday Discuss. 155 (2012) 115−127. https://doi.org/10.1039/C1FD00091H.
[25] Y. Ueda, H. Takeda, T. Yui, K. Koike, Y. Goto, S. Inagaki, O. Ishitani, A Visible-Light Harvesting System for Efficient CO_2 Reduction Using a Supramolecular Ru(II)-Re(I) Photocatalyst Adsorbed in Periodic Mesoporous Organosilica, ChemSusChem 8 (2015) 439−442. https://doi.org/10.1002/cssc.201403194.
[26] C. W. Machan, S. A. Chabolla, J. Yin, M. K. Gilson, F. A. Tezcan, C. P. Kubiak, Supramolecular assembly promotes the electrocatalytic reduction of carbon dioxide by Re(I) bipyridine catalysts at a lower overpotential, J. Am. Chem. Soc. 136 (2014) 14598−14607. https://doi.org/10.1021/ja5085282.
[27] P. L. Cheung, S. C. Kapper, T. Zeng, M. E. Thompson, C. P. Kubiak, Improving photocatalysis for the reduction of CO_2 through non-covalent supramolecular assembly, J. Am. Chem. Soc. 141 (2019) 14961−14965. https://doi.org/10.1021/jacs.9b07067.
[28] L. Q. Qiu, K. H. Chen, Z. W. Yang, L. N. He, A rhenium catalyst with bifunctional pyrene groups boosts natural light-driven CO_2 reduction, Green Chem. 22 (2020) 8614−8622. https://doi.org/10.1039/D0GC03111A.
[29] P. Wang, R. Dong, S. Guo, J. Zhao, Z. M. Zhang, T. B. Lu, Improving photosensitization for photochemical CO_2-to-CO conversion. Natl. Sci. Rev. 7 (2020) 1459−1467. https://doi.org/10.1093/nsr/nwaa112.
[30] T. Chen, M. Li, J. Liu, π–π stacking interaction: a nondestructive and facile means in material engineering for bioapplications. Cryst. Growth Des. 18 (2018) 2765−2783. https://doi.org/10.1021/acs.cgd.7b01503.
[31] A. H. Christopher, K. M. Jeremy, The nature of π–π interactions, J. Am. Chem. Soc. 112 (1990) 5525−5534. https://doi.org/10.1021/ja00170a016.
[32] C. Vriamont, M. Devillers, O. Riant, S. Hermans, Catalysis with gold complexes immobilised on carbon nanotubes by π–π stacking interactions: Heterogeneous catalysis versus the boomerang effect, Chem. Eur. J. 19 (2013)] 12009−12017. https://doi.org/10.1002/chem.201300998.
[33] H. Nasrallah, S. Germain, P. Queval, C. Bouvier, M. Mauduit, C. Crevisy, E. Schulz, Non covalent immobilization of pyrene-tagged ruthenium complexes onto graphene surfaces for recycling in olefin metathesis reactions. J. Mol. Cat. A Chem. 425 (2016) 136−146. https://doi.org/10.1016/j.molcata.2016.10.004.
[34] K. Karami, A. Ramezanpour, M. Zakariazadeh, C. Silvestru, Catalytic activity and facile recovery of a cyclometalated N-heterocyclic carbene palladium (II) complex immobilized by non-covalent interactions on reduced graphene oxide, Appl. Organomet. Chem. 33 (2019) e4907. https://doi.org/10.1002/aoc.4907.

[35] A. Gupta, J. D. Blakemore, B. S. Brunschwig, H. B. Gray, Immobilization and electrochemical properties of ruthenium and iridium complexes on carbon electrodes, J. Condens. Matter Phys. 28 (2016) 094002. https://doi.org/10.1088/0953-8984/28/9/094002.
[36] J. D. Blakemore, A. Gupta, J. J. Warren, B. S. Brunschwig, H. B. Gray, Noncovalent immobilization of electrocatalysts on carbon electrodes for fuel production, J. Am. Chem. Soc. 135 (2013) 18288−18291. https://doi.org/10.1021/ja4099609.
[37] D. W. Thompson, A. Ito, T. J. Meyer, $[Ru(bpy)_3]^{2+*}$ and other remarkable metal-to-ligand charge transfer (MLCT) excited states, Pure Appl. Chem. 85 (2013) 1257−1305. https://doi.org/10.1351/PAC-CON-13-03-04.
[38] D. R. Whang, D. H. Apaydin, S. Y. Park, N. S. Sariciftci, An electron-reservoir Re (I) complex for enhanced efficiency for reduction of CO_2 to CO, J. Catal. 363 (2018) 191−196. https://doi.org/10.1016/j.jcat.2018.04.028.
[39] K. Kalyanasundaram, Photophysics, photochemistry and solar energy conversion with tris (bipyridyl) ruthenium (II) and its analogues. Coord. Chem. Rev. 46 (1982) 159−244. https://doi.org/10.1016/0010-8545(82)85003-0.
[40] S. Y. Li, S. Meng, X. Zou, M. El-Roz, I. Telegeev, O. Thili, T. X. Liu, G. Zhu, Rhenium-functionalized covalent organic framework photocatalyst for efficient CO_2 reduction under visible light, Micropor. Mesopor. Mat. 285 (2019) 195−201. https://doi.org/10.1016/j.micromeso.2019.05.026.
[41] Y. Tamaki, T. Morimoto, K. Koike, O. Ishitani, Photocatalytic CO_2 reduction with high turnover frequency and selectivity of formic acid formation using Ru (II) multinuclear complexes, Proc. Natl. Acad. Sci. 109 (2012) 15673−15678. https://doi.org/10.1073/pnas.1118336109.
[42] B. Gholamkhass, H. Mametsuka, K. Koike, T. Tanabe, M. Furue, O. Ishitani, Architecture of supramolecular metal complexes for photocatalytic CO_2 reduction: Ruthenium− rhenium Bi-and tetranuclear complexes, Inorg. Chem. 44 (2005) 2326−2336. https://doi.org/10.1021/ic048779r.
[43] Y. Tamaki, O. Ishitani, Supramolecular photocatalysts for the reduction of CO_2, ACS Catal. 7 (2017) 3394−3409. https://doi.org/10.1021/acscatal.7b00440.
[44] T. Morimoto, T. Nakajima, S. Sawa, R. Nakanishi, D. Imori, O. Ishitani. J. Am. Chem. Soc. 135 (2013) 16852-16828.
[45] Y. Lu, J. Wang, N. McGoldrick, X. Cui, J. Zhao, C.Caverly, B. Twamley, G. M. Ó Máille, R. M. Conway-Kenny, S. Draper, Iridium(III) complexes bearing pyrene- functionalized 1,10-phenanthroline ligands as highly efficient sensitizers for triplet-triplet annihilation upconversion, Angew. Chem. Int. Ed. 55 (2016) 14688−14692. https://doi.org/10.1002/anie.201608442.
[46] A. D. Becke, Density-functional thermochemistry. III. The role of exact exchange, J. Chem. Phys. 98 (1993) 5648−5652. https://doi.org/10.1063/1.464913.
[47] C. Lee, W. Yang, R. G. Parr, Development of the Colle-Salvetti correlation-energy formula into a functional of the electron density, Phys. Rev. B 37 (1988) 785−789. https://doi.org/10.1103/PhysRevB.37.785.
[48] S. Grimme, J. Antony, S. Ehrlich, H. Krieg, A consistent and accurate ab initio parameterization of density functional dispersion correction (DFT-D) for the 94 elements H-Pu, J. Chem. Phys. 132 (2010) 154104. https://doi.org/10.1063/1.3382344.
[49] A. Schäfer, C. Huber, R. Ahlrichs, Fully optimized contracted Gaussian-basis sets of triple zeta valence quality for atoms Li to Kr. J. Chem. Phys. 100 (1994) 5829−5835. https://doi.org/10.1063/1.467146.
[50] P. J. Hay, W. R. Wadt, Ab initio effective core potentials for molecular calculations. Potentials for K to Au including the outermost core orbitals, J. Chem. Phys. 1985, 82, 299−310. https://doi.org/10.1063/1.448975.